Available online at www.sciencedirect.com
SCIENCE DIRECT®
Journal of Crystal Growth 273 (2004) 220–225
JOURNAL OF CRYSTAL GROWTH
www.elsevier.com/locate/jcrysgro

Czochralski technique growth of pure and rare-earth-doped $SrWO_4$ crystals

Guohua Jia[a,b], Chaoyang Tu[a,b,*], Zhenyu You[a], Jianfu Li[a], Zhaojie Zhu[a], Yang Wang[a], Baichang Wu[a]

[a]*Fujian Institute of Research on the Structure of Matter, Chinese Academy of Sciences, Fuzhou, Fujian 350002, China*
[b]*Graduated School of Chinese Academy of Sciences, 100039, Beijing*

Received 26 June 2004; accepted 30 July 2004
Communicated by M. Schieber
Available online 2 October 2004

Abstract

Pure and rare-earth (Nd^{3+}, Tm^{3+} and Er^{3+})-doped strontium tungstates of good optical quality with sizes of about ϕ20 mm × 50 mm were grown successfully by the Czochralski technique. The (0 0 1) orientation was found to be the favorable direction for crystal growth. X-ray powder diffraction (XRD), differential thermal analysis (DTA) and differential scanning calorimeter (DSC) of pure strontium tungstate were measured. The concentrations of Nd^{3+}, Tm^{3+} and Er^{3+} were measured and their segregation coefficients were also calculated. The absorption and emission spectra of rare-earth-doped crystals as a function of the σ and π polarizations were presented and discussed. Favorable values of the absorption cross section centered at about 800 nm suggest that Nd^{3+}- and Tm^{3+}-doped strontium tungstates are promising candidates for laser diode (LD) pumping.

PACS: 42.70.Hj; 78.20.−e; 81.10.Fq; 65.40.De

Keywords: A2. Czochralski method; A2. Growth from melt; B1. Strontium compounds

1. Introduction

Pure and rare-earth-doped strontium tungstates have received a great deal of interest in the past decades in the fields such as electron paramagnetic resonance [1,2], dielectric properties [3], microstructure [4,5], Raman spectra characteristics [6] and Raman self-conversion media [7]. $SrWO_4$ belongs to the scheelite family; the unit cell parameters are: $a = 5.4168$ Å, $c = 11.951$ Å, $V = 350.66$ Å^3, $z = 4$, $D_c = 6.35\,g/cm^{-3}$ and the space group is $I4_1/a$ [8].

A. Peckter et al. [9], had described the crystallization of $SrWO_4$ crystal from solution in lithium

*Corresponding author. Tel.: +86-591-371-1368/2122; fax: +86-591-371-4946.
E-mail address: tcy@ms.fjirsm.ac.cn (C. Tu).

0022-0248/$ - see front matter © 2004 Elsevier B.V. All rights reserved.
doi:10.1016/j.jcrysgro.2004.07.095

chloride melts. However, a detailed growth method of pure and rare-earth-doped strontium tungstates crystals, to our knowledge, has not yet been reported. In this paper, we present a series of rare-earth-doped strontium tungstate crystals growth from melt by the Czochralski method. Growth methods were presented; measurements of X-ray powder diffraction (XRD) and differential thermal analysis (DTA) were recorded. In addition, polarized absorption and emission spectra of these rare-earth-doped crystals were investigated and assigned to the corresponding transitions.

2. Experimental procedure

The initial chemicals of analytical grade $SrCO_3$, WO_3 and spectral grade Ln_2O_3 (here Ln = Tm, Nd and Er) were mixed separately in the molar ratio in an agate motor and then charged into a platinum crucible. They were heated to 1100 °C and maintained at this temperature for 7 days. After that, the chemicals were deposited in an iridium crucible and were placed in the DJL−400 furnace under nitrogen atmosphere. The compounds were heated

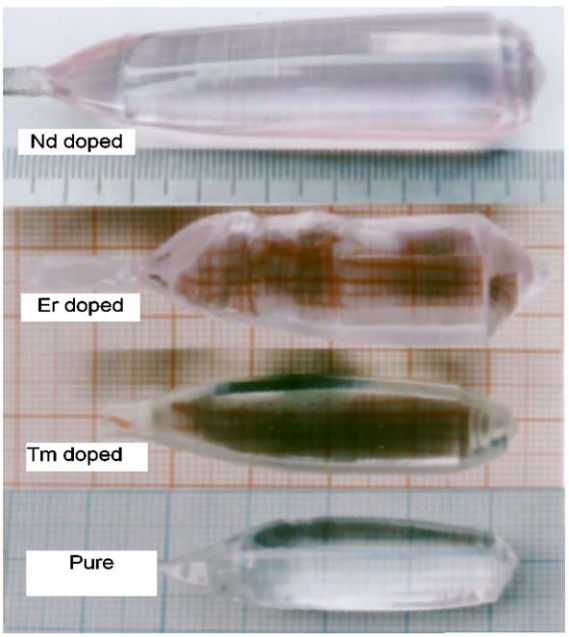

Fig. 1. As-grown pure and rare-earth-doped $SrWO_4$ crystals.

Table 1
Growth parameters of $SrWO_4$ crystals

Parameters	Property	Parameters	Property
Seeding temp. (°C)	1540	Atmosphere	N_2
Soaping temp. (°C)	1590	Pulling rate (mm/h)	1–1.2
Soaping time (h)	2	Rotate rate (rpm)	12–15
Crucible size (mm)	$\varnothing = 50 \times 50$	Annealing rate (°C/h)	12–30
Crucible	Iridium		

Table 2
Properties of pure and rare-earth-doped $SrWO_4$ crystals

Crystals	Size	Color	Ions concentration (10^{19}/cm^3)	Segregation coefficient (%)
Pure $SrWO_4$	40×12	Colorless	—	—
Nd^{3+}:$SrWO_4$	60×20	Sky-blue	8.5	20.09
Er^{3+}:$SrWO_4$	50×20	Red	8.0	20.28
Tm^{3+}:$SrWO_4$	50×15	Colorless	6.2	15.78

to a temperature of 50 °C higher than the crystallization temperature for about 2 h to allow the melt to mix completely and homogeneously. Pure $SrWO_4$ seed was selected from small crystals obtained by spontaneous crystallization and was used to grow bulky $SrWO_4$ crystal. The seeds used in the subsequent experiments were oriented parallel to the *c*-axis. The rotate and pulling rates were 12–15 rpm and 1–1.2 mm/h, respectively. When these procedures were over, the crystals were drawn out of the melt and cooled down to room temperature at a rate of 12–30 °C/h. Grown crystals are shown in Fig. 1 and the growth parameters are displayed in Table 1.

The rare-earth ions concentrations were measured by the ICP–AES method. Nd^{3+}, Er^{3+} and Tm^{3+} concentrations of these crystals were 0.33, 0.31 and 0.24 at%, respectively. The effective coefficients were determined by the following formula:

$$K_{Ln} = \frac{(\text{molesLn}/(\text{molesLn} + \text{molesSrWO}_4))_{\text{crystal}}}{(\text{molesLn}/(\text{molesLn} + \text{molesSrWO}_4))_{\text{melt}}}.$$

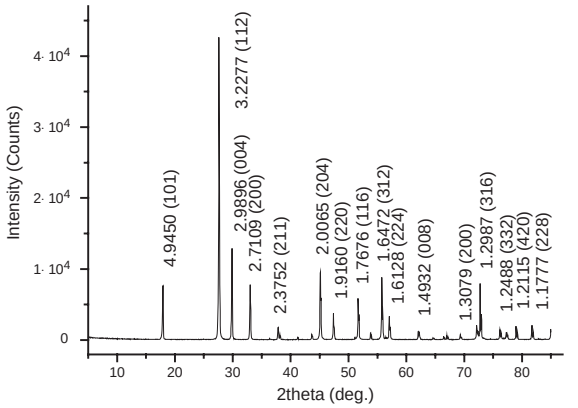

Fig. 2. XRD of a pure $SrWO_4$ crystal.

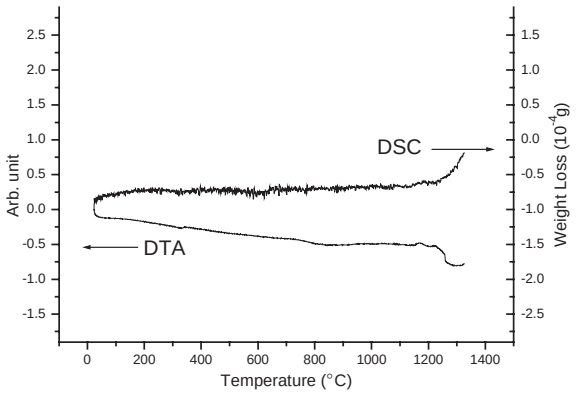

Fig. 3. DTA and DSC graphs of a pure $SrWO_4$ crystal.

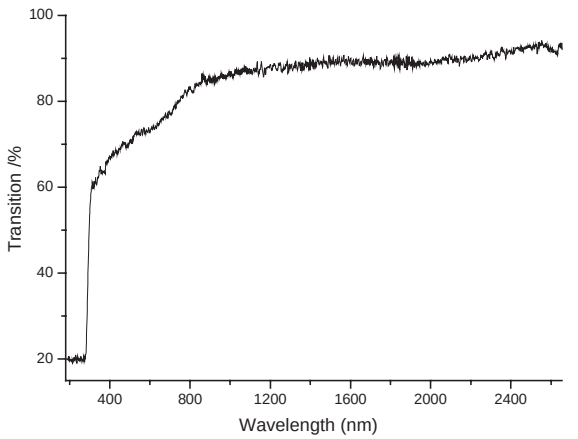

Fig. 4. Transmission spectrum of a pure $SrWO_4$ crystal recorded at room temperature.

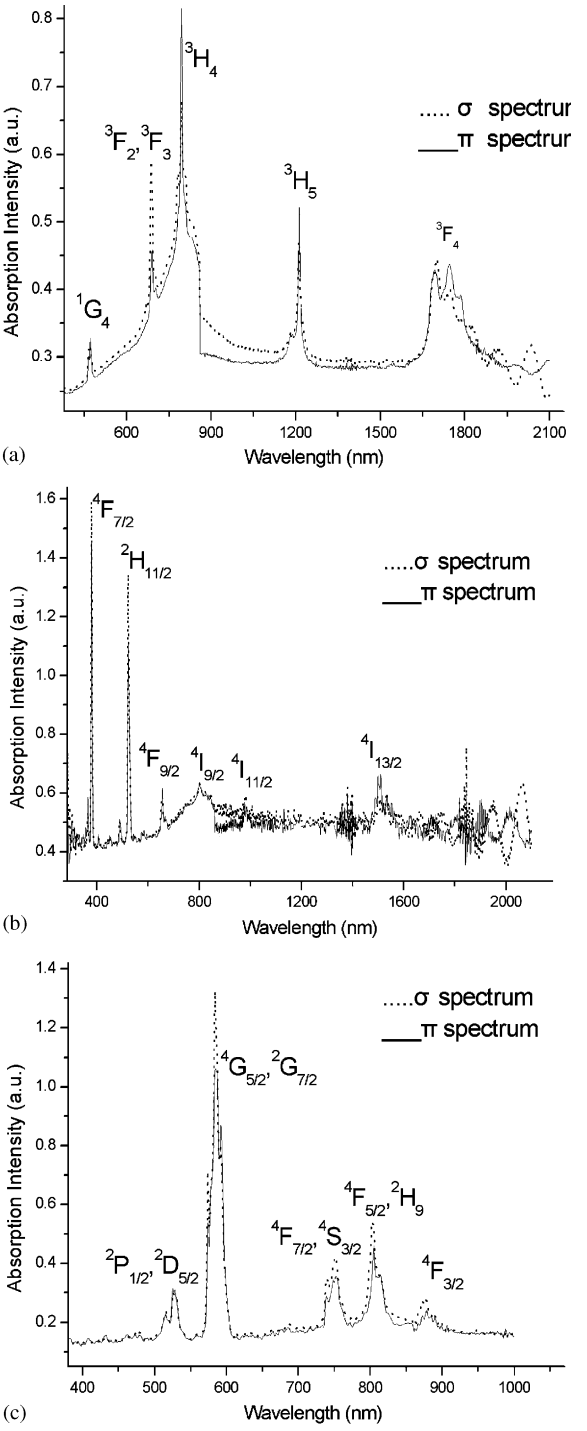

Fig. 5. Absorption spectra recorded at room temperature (a) Tm^{3+}:$SrWO_4$, (b) Nd^{3+}:$SrWO_4$, (c) Er^{3+}:$SrWO_4$.

Here Ln is the lanthanide such as Nd^{3+}, Tm^{3+} and Er^{3+}. Table 2 presents the properties of these pure and rare-earth-doped $SrWO_4$ crystals.

XRD investigations were carried out with a CAD4 diffractometer equipped with CuK α radiation ($\lambda = 1.054056$ Å). The data were collected using a Ni-filtered Cu-target tube at room temperature in the 2θ range of 5°–85°. Fig. 2 shows the XRD patterns of a pure $SrWO_4$ single crystal. The XRD pattern was in good accordance with the standard XRD powder card of $SrWO_4$.

DTA and differential scanning calorimeter (DSC) graphs were measured by Netzsch STA449C in the temperature range of 30–1300 °C in a N_2 atmosphere at heating rates of 10 °C/min (shown in Fig. 3). On the heating curve, there was only one endothermic peak (1300 °C) of the DTA curve corresponding to the weight loss of the DSC curve. This may be a result of the sublimation of the extra WO_3 in the sample; a similar phenomenon was also found for $La_2(WO_4)_3$ and $Sm_2(WO_4)_3$ crystals [10,11]. Thus, there is no high-temperature phase transition in the range of 30–1320 °C for $SrWO_4$ crystal.

3. Spectrum characteristics

Room temperature transmission and absorption spectra of these crystals were recorded by a Perkin–Elmer UV–VIS–NIR Spectrometer (Lambda-35). The transmission spectrum of a pure $SrWO_4$ crystal is shown in Fig. 4. It is transparent up to 2700 nm and its ultraviolet absorption edge is at 300 nm. This broad transmission range enables the study of rare-earth ion transitions in the visible and infrared region.

Fig. 5 (a), (b) and (c) presents Tm^{3+}-, Nd^{3+}- and Er^{3+}-doped $SrWO_4$ crystals polarized absorption spectra recorded at room temperature. Each absorption band was assigned to the corresponding transitions from the ground state of Tm^{3+}, Nd^{3+} and Er^{3+}, respectively. The most interesting aspects of the absorption spectra in Fig. 5 (a) and (b) were the intensive absorption bands at about 800 nm, which were suitable for pumping of commercial GaAlAs laser diode. The FWHM of the σ and π spectra absorption peak of Tm^{3+}:$SrWO_4$ crystal at about 795 nm is about 10 and 7 nm, respectively. As for Nd^{3+}: $SrWO_4$ crystal, the σ spectra absorption peak is at 801 nm and the FWHM is 17 nm while the the π spectra absorption peak is at 805 nm and the FWHM is 14 nm.The absorption cross section σ_a can be determined by the following equation:

$$\sigma_a = \alpha/\mathrm{Nc},$$

where α is the absorption coefficient, $\alpha = A/L \log e$, A is the absorbance, L is the thickness of the polished crystal, and Nc is the rare-earth ions concentration in atoms. The absorption cross section of Tm^{3+}:$SrWO_4$, Nd^{3+}:$SrWO_4$ and other crystals are compared in Table 3. The moderate absorption cross sections and the larger FWHM indicate that Tm^{3+}:$SrWO_4$ and Nd^{3+}:$SrWO_4$

Table 3
Comparison between the FWHM and absorption cross section in Tm^{3+}- and Nd^{3+}-doped crystals

Crystals	Polarization spectra	Wavelength (nm)	FWHM (nm)	Cross section (10^{-20} cm^2)	Ref.
5 at% Tm:YVO_4	π	797.5	5	2.5	[12]
0.5 at% Tm:$LiTaO_3$	σ	795	9.5	6	[13]
0.7 at% Tm:$KYb(WO_4)_2$	π	793.6	3.5	8.8	[14]
	σ	801.8	1.4	4.8	
0.24 at% Tm:$SrWO_4$	π	795	7	7.01	This work
	σ	795	10	5.83	
1.5 at% Nd^{3+}:$Gd_{0.8}La_{0.2}VO_4$	π	808.5	6.2	14.74	[15]
3.81 wt% Nd^{3+}:LaB_3O_6	Unpolarization	799	16	3.37	[16]
0.33 at% Nd:$SrWO_4$	π	805	14	4.46	This work
	σ	801	17	4.48	

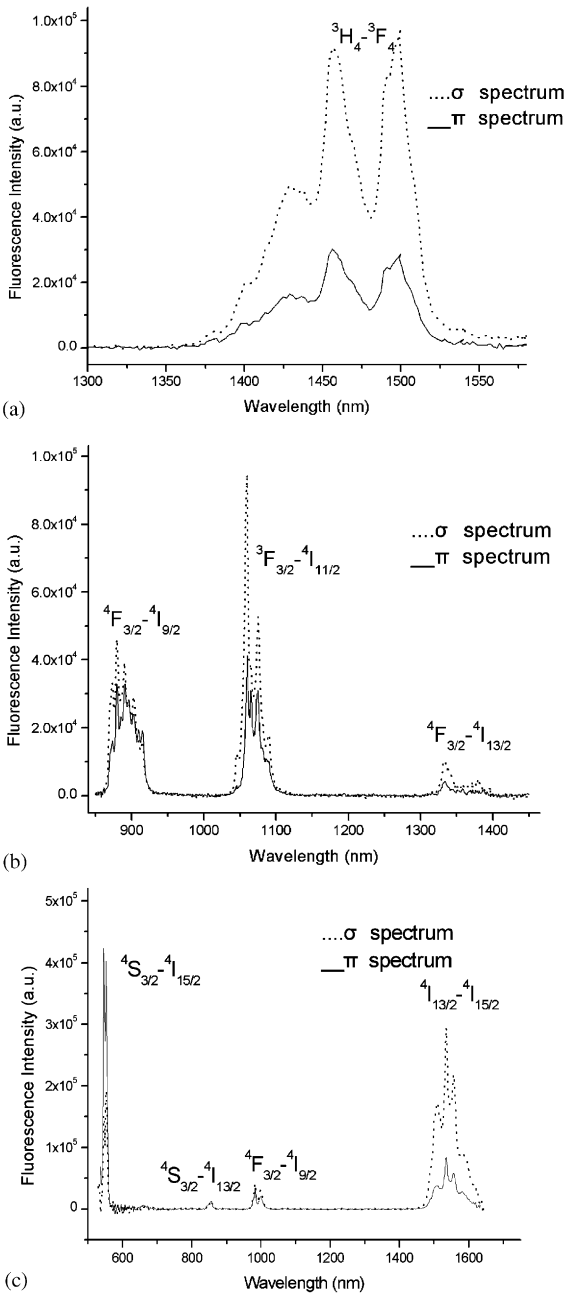

Fig. 6. Emission spectra recorded at room temperature (a) Tm^{3+}:$SrWO_4$ (805 nm pumping), (b) Nd^{3+}:$SrWO_4$ (805 nm pumping) and (c) Er^{3+}:$SrWO_4$ (521 nm pumping).

crystals are preferable to be pumped by the GaAlAs laser diode.

Polarized emission spectra of these crystals were recorded at room temperature by using an Edinburgh Instruments FLS920 spectrophotometer (shown in Fig. 6). Each emission band was also assigned to the corresponding transitions between the inter-levels of these rare earth ions. In Fig. 6 (a), (b) and (c) the intense emission peaks are centered at 1457 nm, 1061 nm and 1536 nm corresponding to the transition $^3H_4$–$^3F_4$ of Tm^{3+} ions, the transition $^3F_{3/2}$–$^4I_{11/2}$ of Nd^{3+} ions and the transition $^4I_{13/2}$–$^4I_{15/2}$ of Er^{3+} ions, respectively. In addition, the intensity of σ emission spectra was much stronger than that of π emission spectra, indicating larger dependence of the emission spectra on polarization.

4. Results and Discussions

Transparent and crack free of pure and rare-earth (Tm^{3+}, Nd^{3+} and Er^{3+})-doped $SrWO_4$ crystals were grown successfully by the Czochralski technique. A pure $SrWO_4$ crystal was grown by spontaneous crystallization along the *b*-axis direction, while Tm^{3+}-, Nd^{3+}- and Er^{3+}-doped $SrWO_4$ crystals were grown along the *c*-axis orientation. Crystals grown along the *b*-axis were more easily cracked than those grown along *c*-axis directions; thus the (0 0 1) orientation should be the favorable direction. This result was in good accordance with the growth properties of $BaWO_4$ crystals reported in Ref. [17]. In addition, both comparative lower pulling rates and suitable annealing program also contributed to the cracking free of these crystals.

We presented polarized absorption and emission spectra of rare-earth (Tm^{3+}, Nd^{3+} and Er^{3+})-doped $SrWO_4$ crystals. Results showed that there were hardly any differences between the π polarized and the σ polarized absorption spectra, which implied that the absorption spectra showed little depended on the polarization. On the contrary, the intensity of σ polarized emission spectra was much stronger than that of the π polarized emission spectra, indicating high dependence of the emission spectra on the polarization.

We measured the FWHM and calculated the absorption cross section centered at about 800 nm of Tm^{3+}- and Nd^{3+}-doped $SrWO_4$ crystals. Favorable values of FWHM and absorption cross-section suggest that Tm^{3+}:$SrWO_4$ and Nd^{3+}:$SrWO_4$ crystals are promising candidates for LD pumping.

Acknowledgement

This project was supported by the Natural Science Foundation of China and the Natural Science Foundation of the Fujian Province of China (2002I016) and (2001H107).

References

[1] J. Bronstein, S. Maniv, Phys. Rev. 153 (1967) 303–306.
[2] J.P. Sattler, J. Nemarich, Phys. Rev. B 1 (1970) 4249–4256.
[3] W.S. Brower, JR., P.H. Fang, J. Appl. Phys. 40 (1969) 4988–4989.
[4] Woo-Seok Cho, Masatomo Yashima, Masto Kakihana, Akihiko Kudo, Tadayoshi Sakata, Masahiro Yashimura, J. Am. Ceram. Soc. 78 (1995) 3110–3112.
[5] J.Y. Huang, Q.X. Jia, Thin Solid Films 444 (2003) 95–98.
[6] S.P.S. Porto, J.F. Scott, Phys. Rev. 157 (1967) 716–719.
[7] L.I. Ivleva, T.T. Basiev, I.S. Boronina, P.G. Zverev, V.V. Osiko, N.M. Polozkov, Opt. Mater. 23 (2003) 439–442.
[8] Erdogan Gurmen, Ergene Daniels, J.S. King, J. Chem. Phys. 5 (1971) 1093–1097.
[9] A. Pachter, B.N. Roy, J. Crystal Growth 18 (1973) 86–93.
[10] Xiaoding Qi, Zundu Luo, Jingkui Liang, J. Crystal Growth 246 (2000) 363–366.
[11] L.H. Brixner, A.W. Sleight, Mater. Res. Bull. 8 (1973) 1269.
[12] Kei Ohta, Hideaki Saito, Minoru Obara, J. Appl. Phys. 73 (1993) 3149–3152.
[13] I. Sokolska, W. Ryba-Romanowski, S. Golab, M. Baba, M. Swirkowicz, T. Lukasiewicz, J. Phys. Chem. Soli. 61 (2000) 1573–1581.
[14] M.C. Pujol, F. Guell, X. Mateos, Jna. Gavalda, R. Sole, J. Massons, M. Aguilo, F. Diaz, G. Boulon, A. Brenier, Phys. Rev. B 66 (2002) 144304.
[15] H.D. Jiang, J.Y. Wang, H.J. Zhang, X.B. Hu, H. Liu, J. Appl. Phys. 92 (2002) 3647–3650.
[16] Guohua Jia, Chaoyang Tu, Zhenyu You, Jianfu Li, Baichang Wu, J. Crystal Growth 266 (2004) 492–495.
[17] A.K. Chauhan, J. Crystal Growth 254 (2003) 418–422.